

PROCEEDINGS OF SPIE

[SPIEDigitallibrary.org/conference-proceedings-of-spie](https://spiedigitallibrary.org/conference-proceedings-of-spie)

Recent trends in hard X-ray tomographic imaging

Bert Müller

Bert Müller, "Recent trends in hard X-ray tomographic imaging," Proc. SPIE 12242, Developments in X-Ray Tomography XIV, 1224202 (22 November 2022); doi: 10.1117/12.2625223

SPIE. Event: SPIE Optical Engineering + Applications, 2022, San Diego, California, United States

Recent trends in hard X-ray tomographic imaging

Bert Müller^{*a,b}

^aBiomaterials Science Center, Department of Biomedical Engineering, University of Basel, 4123 Allschwil, Switzerland; ^bBiomaterials Science Center, Department of Clinical Research, University Hospital Basel, 4031 Basel, Switzerland

ABSTRACT

Several thousand X-ray computed tomography systems are currently operated in clinics, industry, and academia. While conventional attenuation-based imaging is still dominant, alternative and complementary contrast mechanisms are under development and already in use. The generated big datasets require state-of-the art methods for image reconstruction, artefact removal, and analysis. Several technical advancements are enabling or pushing applications of tomography in pathology, tissue engineering, anthropology, *etc.* It is common to produce impressive imagery of unique objects and derive relevant features of the underlying structures and dynamics. Multi-modal imaging, which includes synergistic and reciprocal information, has played an increasing role. This interdisciplinary field comprises researchers and users from medicine/dentistry, biology, earth and materials science, crystallography, solid-state and soft-matter physics, chemistry, computational sciences, engineering, and applied mathematics to fruitfully combine results on system and component developments, algorithmic design and optimization, performance evaluation, and tomography experiments. This paper summarizes key aspects of the 55 contributions in the 14th volume on *Developments in X-ray Tomography*, arranged in sections on instrumentation, algorithms, and applications.

Keywords: Computed tomography, phase tomography, microtomography, nanotomography, synchrotron radiation, image analysis, artificial intelligence, multimodal imaging.

1. INTRODUCTION

In research, laboratory- and synchrotron radiation-based tomography systems are currently used for non-destructive visualization of micro- and nano-structures [1]. The obtained three-dimensional data of unique objects and biological tissues represent physical quantities related to the local X-ray absorption coefficients, the local electron densities and their combination.

Instrumentation for micro- or even nanometer resolution consists of at least a source, precision a rotation stage, and a detection unit [1]. The choice of instrumentation and imaging protocol is critical for successful visualization of the features of interest. The success also crucially depends on object preparation and handling. Nevertheless, the raw data are often noisy and contain a variety of artefacts. Consequently, computational sciences are required to obtain the desired quality of imaging data. Manual approaches, if still in use, are generally replaced by more or less sophisticated automatic processing steps.

Alternatives to conventional, purely attenuation-based tomography include phase tomography, spectral imaging and three-dimensional reciprocal-space techniques. These approaches count on recent advances in X-ray source developments and detector technologies. The valid comparison of the high-resolution tomography systems is object-dependent [2] and includes quantitative characterization of the X-ray sources, the stability of the rotation stages, the dynamic range and pixel sizes of the imaging devices as well as an assessment of image quality. The impact of the image-processing filters implemented in reconstruction and artifact compensation is usually underestimated. Their selection should be simple. Finally, manual approaches are often more time-consuming than fully automatic procedures to extract the features of interest and to register the tomography data with two- or three-dimensional datasets for multi-modal imaging [3].

*bert.mueller@unibas.ch; phone +41 61 207 5430; fax 41 61 207 5499; www.bmc.unibas.ch

This proceedings volume contains almost 50 papers. SPIE's Digital Library lists 39 contributions with both presentation and paper, two contributions with paper only, and eight presentation-only contributions. Figure 1 shows the number of contributions to the conference series "Developments in X-ray Tomography". The 54 contributions can be grouped into three pillars, *i.e.* hard X-ray tomography instrumentation, algorithms for reconstruction, artefact removal and data treatment, as well as applications of the technique relevant in medicine and beyond.

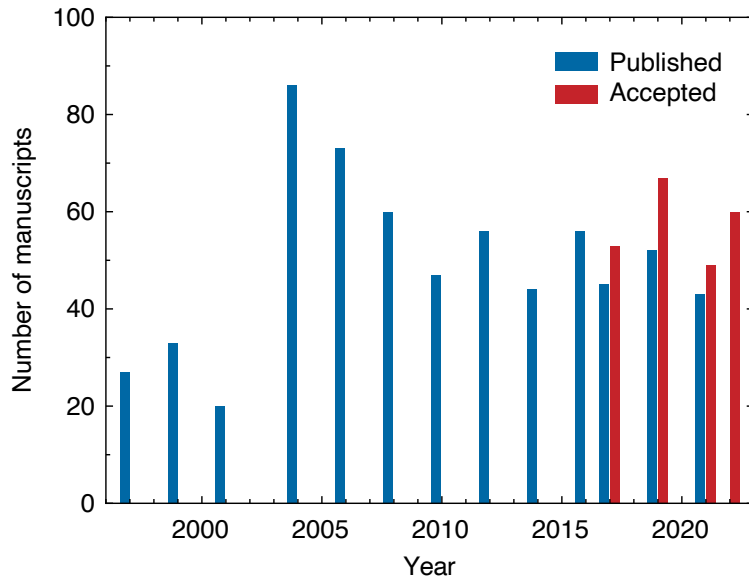


Figure 1. Ulrich Bonse initiated the conference series on *Developments in X-ray tomography* in 1997. He successfully chaired the conference five times. Subsequently, Stuart R. Stock chaired the conference five times between 2008 and 2016. Ge Wang and the author have cooperatively organized the last four events in the years 2017, 2019, 2021, and 2022. This year, we accepted 66 contributions, and 60 talks and posters were finally presented.

2. EVOLUTION OF INSTRUMENTATION FOR X-RAY TOMOGRAPHY

2.1 Alternative and complementary contrast mechanisms

A. Schropp *et al.* introduced the ptychographic nano-analytical microscope (PtyNAMi), is located at beamline P06 at the synchrotron radiation source PETRA III (DESY, Hamburg, Germany) [4]. The three-dimensional structural distribution of a nickel sample was retrieved with a spatial resolution close to 50 nm. The current resolution limits were attributed to the stability and inaccuracies of the experimental setup [4]. Synchrotron radiation sources of the fourth generation, including the planned PETRA IV source, might push the resolution below 10 nm [4].

A. Doherty *et al.* elucidated the power of dark-field tomography for a tissue-engineered esophagus, a pouch cell battery and a fiber-reinforced composite [5]. As the ultra-small angle X-ray scattering signal linearly scaled with sample thickness, the acquired data could be reconstructed through a standard reconstruction algorithm [5].

M. Liebi has combined small-angle X-ray scattering with raster-scanning bone through the beam. To extend the approach to computed tomography, reconstruction algorithms and experimental setups probing additional tilt angles were developed [6]. In bone, the arrangement of mineralized collagen fibrils could be probed over millimeters [6].

Similarly, C. Appel *et al.* [7] characterized nano-porous composites over multiple length scales on a fuel cell catalyst. The imaging data comprised direct images of the nano-pores in a 30 μm -thick catalyst pillar. This material study was complemented by the three-dimensional imaging of vapor condensation with 20 nm resolution in time steps of ten minutes [7].

2.2 Advanced tomography using synchrotron radiation

Synchrotron radiation sources, including the Advanced Photon Source at Argonne National Laboratory, have been made more efficient by combination with smart and fast detection units. V. Nikitin impressively illustrated real-time tomographic imaging at beamline 2-BM with automatic zooming to features of interest in a highly efficient fashion [8].

The Helmholtz-Zentrum Hereon, Germany, made similar progress in optimized X-ray detection. F. Beckmann *et al.* [9] highlighted the need of dose optimization especially for biological samples. He summarized the related measures, *i.e.* the integration of dedicated imaging detectors in combination with a high-speed shutter for the X-ray triggering [9]. The focus was on the beamline P07 at the synchrotron radiation source PETRA III (DESY, Hamburg, Germany) [9].

To further improve the data acquisition schemes used for tomographic imaging at the beamlines P05 and P07 at the synchrotron radiation source PETRA III (DESY, Hamburg, Germany), B. Kazimi *et al.* developed algorithms for satisfying segmentation using a minimum number of slices [10].

N. Vo *et al.* implemented speckle-based phase-retrieval methods at the Diamond Light Source [11]. This open-source Python software is available for the entire community. The authors showed that (i) the 1D-search method has been particularly helpful for users without access to GPU, (ii) the dark-signal image retrieved has been supportive for applications, and (iii) the low-pass component of phase-shift image has been varied depending on surface-reconstruction method and boundary conditions [11].

S. Ahmed explained the DIAD beamline at Diamond Light Source [12]. It is a dual-beam instrument for combined full-field imaging and powder diffraction. The two independent X-ray beams with photon energies between 8 and 38 keV allows for microtomography with a field-of-view of 1.4 mm × 1.2 mm [12].

2.3 Progress in three-dimensional imaging

M. Li *et al.* designed a robotic-arm-based photon-counting microtomography system for bone imaging with a spatial resolution of 50 µm [13]. The two robotic arms carried a microfocus source and a photon-counting detector to flexibly scan any volume of interest. This system is featured by data-driven imaging geometric calibration with a locally linear embedding-based motion correction method [13]. The calibration method, built on a parametric searching mechanism through iterative reconstruction, is the key for their interior tomography results with substantially improved anatomical details [13]. We can reasonably expect more applications of this imaging approach in biomedical and industrial applications.

The Monte-Carlo simulation of P.-J. Vanthienen *et al.* [14] was focused on the optimization of the grating geometry for cone-beam phase tomography. The study included curved, sheared, and folded gratings. From the perspective of applications, folded gratings, which were based on conventional gratings, could be aligned as conventional ones. Sheared gratings can be positioned to easily permit simple phase stepping.

A. Momose *et al.* pushed the spatial resolution limits of phase imaging with grating interferometers [15]. For this purpose, they built two laboratory-based apparatuses. One instrument combined a commercially available Fresnel zone plate-based X-ray imaging microscope and Lau interferometer optics. The other was a sub-period-resolution X-ray phase imaging device, based on the sample-scanning scheme across the beamlet array formed by a triangular phase grating. The proof-of-concept results demonstrated a spatial resolution better than the period of the gratings [15].

M. Bech proposed a modification of the binary gratings with alternating regions of shift and no shift [16]. He simulated the use of multiple binary structures in the phase grating taking advantage of Moiré effects. The simulations indicated that the Moiré frequency beating translated into an intensity modulation of corresponding low spatial frequencies [16]. The proposition of such a modification might have a major impact on virtual histology of tissue biopsies by means of laboratory-based systems with microfocus X-ray sources.

A. Yoneyama demonstrated that a crystal-based X-ray interferometer can be used for three-dimensional temperature measurements in water or food flow [17]. The preliminary data showed a temporal resolution of 1.3 s and a temperature sensitivity of 2 K [17]. Interesting applications of this system lie in several fields such as battery research [18].

2.4 Protocols for system augmentation

A team from Belgium optimized the design and the positioning of two gratings in a laboratory-based tomography system to perform phase tomography [19]. The simulations J. Sanctorum *et al.* yielded 100 μm pitches and 20 μm apertures for the sample grating, whereas the detector grating should have 148 μm pitches and 30 μm apertures [19].

In a preliminary simulation study aimed at container inspection, C. Bossuyt *et al.* proposed multiple static X-ray sources, a configuration to be optimized with respect to position and orientation [20]. They challenged the equidistant distribution of X-ray sources as the preferred configuration and compared the reconstructions with those of a projected circular distribution [20].

Radiographs are not only used in container inspection but also in medical imaging. C. Niu *et al.* proposed collaborative detection networks for lung nodule imaging, a technique termed X-ray dissection [21]. The simulation-augmented experimental results showed the improved lung nodule detection performance. The authors have planned a dose-efficient diagnosis of lung diseases on the basis of multi-angle radiographs [21].

S. Karimi and J. Tringe studied an underestimated phenomenon in X-ray detection, *i.e.* the impact of cross-talk on the spatial resolution [22]. They experimentally benchmarked their analytical model by measuring the spatial resolution with a tungsten wire 50 μm in diameter on a flat-panel detector [22].

3. DEVELOPMENTS OF ALGORITHMS FOR TOMOGRAPHIC IMAGING AND ANALYSES

3.1 Image Reconstruction

B.P. Patil *et al.* proposed a powerful method to compensate for low-performing detector pixels [23]. They applied deep learning to correct the pixel information in the sinogram domain and showed substantial improvement over other interpolation approaches [23]. Their approach used complimentary information including neighboring row information and conjugate information that is adaptive to local statistics and anatomy, associated with an improved performance over analytical methods [23].

Q. Gao and H. Shan introduced low-dose image denoising based on a diffusion model [24]. The approach used the residual image as the initial input for the forward process. The model was trained to gradually degenerate this residual image to a Gaussian distribution. The contextual information of adjacent slices was also exploited for noise estimation to restore structural details in full-dose images [24].

Low-dose denoising is also the focus of the study by C. Niu *et al.* [25]. In this study, they presented the self-supervised dual-domain network denoising. The training process avoided the use of clean and noisy reference images so that it can be applied to process clinical images [25]. The self-supervised dual-domain network could be improved using advanced networks, and further optimized and tested on big datasets [25].

3.2 Image quality enhancement

A research team at the P05 imaging beamline at PETRA III at DESY, Hamburg, Germany, could offer full-field nanotomography with a spatial resolution of 50 nm and below [26]. They integrated a transmission X-ray microscope with Zernike phase contrast and near-field holotomography for users from biology, materials science, and medicine [26].

Ptychographic X-ray computed tomography also reached nanometer resolution and avoided X-ray optics. S. Achilles *et al.* successfully combined ptychographic reconstruction algorithms with tomographic reconstruction [27]. They demonstrated that their performance was strongly correlated to the dimensions of the reconstructed volume, the size of the diffraction patterns, and the applied tomographic reconstruction algorithm. As an example, they showed a zeolite dataset that was generated with one coupled ptychographic tomography iteration in seconds, fast enough to allow for data analysis in real time [27].

Authors from the company Carl Zeiss X-ray Microscopy proposed a workflow for automated resolution recovery using a combination of multiscale imaging, automated registration, and artificial intelligence-based point-spread-function deconvolution [28]. The approach was benchmarked imaging a tomato seed, a cathode particle, and a chip. For these objects the image quality was substantially improved [28].

N. Six *et al.* [29] presented a joint reconstruction method for edge illumination data that yielded attenuation, refraction, and dark-field tomograms, simultaneously. They studied step size choices in gradient descent and concluded that the use of a split Barzilai-Borwein scheme could be better than the standard Barzilai-Borwein scheme or Armijo line searches in terms of convergence speed and reconstruction quality [29].

S.Z. Li *et al.* applied deep learning for phase retrieval with the aim to reduce the dose in clinical settings [30]. They assumed that the radiation exposure is proportional to the number of images taken and concluded that their approach would reduce the dose by almost a factor of two [30].

3.3 Efficient algorithms for quantification

Image registration has been of key importance to exploit tomography data, cf. for example ref. [31]. C. Tanner *et al.* [32] provided an overview of image registration algorithms with a focus on the challenges related to weak image features, complex appearance changes via embedding procedures, large shape changes including feature-dependent shrinkage, and huge images.

A. Tekawade *et al.* [33] discussed the application of synchrotron radiation-based microtomography for porosity measurements. They developed and implemented a porosity mapping code that could process the recorded radiographs into a porosity measure and visualize them within minutes [33].

Fibers can be thinner than the spatial resolution of a tomography system, but their orientation could be extracted from the dark-field data [34]. This method formed the basis of the computational study of B. Huyge *et al.* [35], who expanded the approach by adding constrained spherical deconvolution as a transformation from the measured scattering function to the fiber orientation distribution.

P. Paramonov *et al.* [36] presented three approaches to simulate X-ray projections from triangular meshes. One approach was based on rasterization and the other two on ray tracing. They also described their implementation and applicability to phase tomography.

3.4 Artifact compensation

A research team from industry considered an empirical beam-hardening correction algorithm applied to metal artifact reduction in cone-beam microtomography [37]. The algorithm basically consisted of segmenting metal components out of uncorrected image data, forwarding projection to create metal only projection data, and creating correction basis images. The algorithm was benchmarked using a cable connector and shaving razor with five primary blades [37].

Full-field nanotomography requires objects with a diameter below one millimeter. Their placement on the holder can be tricky. M. Li *et al.* [38] gave an example: a part of a sea urchin tooth was glued on a metallic pin. This pin resulted in streak artefacts, which could be greatly suppressed by iterative reconstruction with simple metal-trace masked from a regular scan of an imperfectly mounted specimen [38].

A.T. Nguyen *et al.* [39] presented a method to simultaneously reconstruct an image from a moving object and estimated the corresponding motion parameters. The method yielded similar results to established approaches without nested iterations or finite differences approximations [39].

Diagnosing and monitoring cardiovascular diseases on the basis of tomography data is challenging because of unpredictable motion artefacts. A. Sushmit *et al.* proposed a pipeline for building a benchmark dataset that accounted for anatomical, physiological, and pathological variations in data along with scanner type and reconstruction algorithm [40]. They demonstrated the merits of their approach and provided a guideline for ensuring source-agnostic representation of anatomical and pathological imaging biomarkers in cardiac CT applications [40].

4. CUTTING-EDGE APPLICATIONS OF COMPUTED TOMOGRAPHY

4.1 Trends in X-ray tomography with focus on stains

For decades, scientists and engineers have searched for staining materials and imaging protocols for the visualization of the entire vasculature of mice. So far, the success was limited because of clustering and non-stained water and gas inclusions. W. Kuo *et al.* [41] made available a patented water-soluble compound that inherently avoided aggregation and inclusions. They described the rationales, processes, and challenges involved in creating the contrast agent [41].

T. Dreier *et al.* [42] searched for vessel staining to be used for laboratory-based phase-contrast microtomography with 25 μm -wide voxels. They could tune the stain concentration to prevent beam-hardening artefacts [42]. The results were benchmarked against histology [42].

J. Reichmann *et al.* [43] showed that neodymium acetate could penetrate the murine eye uniformly and therefore increased contrast and resolution at the central nervous system down to the cyto-architectural level. Although the murine retina in whole-eye preparations was only a very specific example, the predicted experimental result demonstrated the suitability of neodymium acetate for phase tomography [43].

K. Taphorn *et al.* [44] investigated the standard deviation in basis material images for the quantitative investigation of X-ray stains in ptychographic computed tomography for selected heavy elements. They found that (i) for more electron dense materials the decomposition generally had lower noise in the basis material image of the stain, (ii) especially for materials with low atomic number, the lowest possible X-ray energy should be selected and (iii) for K-edge materials, a photon energy above the K-edge was favorable [44].

4.2 Mechanically loaded tissues and materials

M. Humbel *et al.* [45] studied dental filling materials that could adapt the color of the surrounding enamel. The team demonstrated how tomographic imaging using a transmission X-ray microscope could be employed to visualize the mesoscopic structures of such dental resin composites [45]. For a selected product, this structural information was combined with a Monte Carlo simulation to show the dependence of the spectral transmittance on the composition, structure and arrangement of spherical filler particles [45].

J. von Jackowski *et al.* [46] studied a unique mummy tooth with the aim to identify annual layers in the cementum. Laboratory-based microtomography supported the discrimination between enamel, dentin, and cementum, but the annual layers became only visible by means of the synchrotron radiation-based tomography system [46]. Up to 35 layers with an average thickness of $(4.6 \pm 1.4) \mu\text{m}$ were identified using a specific pipeline further developed in this study [46].

A.A. Velasco *et al.* [47] studied cementum deposits on bovid teeth, which showed layered microstructures associated with age. Such layers were identified in teeth from gemsbok, eland, and buffalo [47]. Thus, the physical sectioning to obtain slices for optical microscopy could be avoided.

S.R. Stock *et al.* [48] used synchrotron radiation-based microtomography and also found such layered deposits for age determination in the spines of dogfish. This three-dimensional mapping also allowed for studying the microstructural origin of the band contrast by combination with X-ray excited X-ray fluorescence [48]. As found in growth bands in other mineralized tissues, the modulation could be related to the zinc content [48].

4.3 Imaging biological cells in tissue context

Joint tissues consist of bone and cartilage with varying density, which presents a challenge for tomographic imaging due to the wide range of local X-ray absorption values. Therefore, G. Schulz *et al.* [49] decalcified a surgically treated porcine joint and imaged the entire joint in ethanol with a laboratory-based system. Biopsies of selected parts were visualized for the imaging of chondrocytes and consequently for the differentiation between the cartilage types by means of synchrotron radiation-based microtomography and benchmarked against the gold standard histology [49].

The performance of tomographic imaging can be perfectly demonstrated by the cochlea, a rather complex three-dimensional anatomical structure [50]. The anatomy of the cochlea is crucial to understand its functionality [51] and

developments [52, 53] as well as to design inner ear implants [54]. J.J. Schaeper, M.C. Liberman, and T. Salditt [55] presented phase tomography data of cochleae from Guinea pigs and humans acquired at synchrotron radiation facilities and a laboratory source. Whereas heavy metal stains were beneficial at the laboratory setup, the contrast of unstained cochleae at the synchrotron radiation facility was sufficient for cellular resolution [55].

M. Riedel *et al.* visualized the vascular system of murine lymph nodes down to 5 μm -wide capillaries using Talbot array illuminators at the beamline P05, PETRA III at DESY, Hamburg, Germany [56]. The team compared resin-embedded and ethanol-immersed tissues in hematein-lead-stained and unstained stages. The resin embedding was preferred, because movement was prevented, although the signal-to-noise ratio was compromised [56]. The staining accentuated the node and the follicles [56].

J. Romell *et al.* used hard X-ray phase tomography to complement conventional histology with the aim to determine the interface between cancerous and healthy tissues in soft tumors in three dimensions with reasonable precision [57]. Because this analysis should be applied in direct neighborhood to the operating room, they have performed the imaging experiments with the laboratory-based phase tomography setup, which contained a liquid metal jet X-ray source [57].

G. Rodgers *et al.* acquired an entire mouse brain with a volume of 450 mm^3 using 0.65 μm -wide voxels, which gave rise to a tera-voxel-sized dataset [58]. It was obvious that both the acquisition protocol and the treatment of the big data needed attention. The team showed that mosaic tiling extended the imaged volume by a factor of 400 [58]. The dataset with 6 TB in size at 16-bit depth contained the sub-cellular anatomy of the entire mouse brain to be segmented [58] and will be publicly available.

4.4 Challenging research questions

L. Croton *et al.* demonstrated that phase tomography could resolve anatomical microstructures within the brains of small animals [59] and developed an artifact correction method for soft tissue imaging inside the skull [60]. Now, L. Croton *et al.* used this knowledge to detect brain injury in direct comparison with magnetic resonance imaging [61].

T. Partridge *et al.* [62] presented phase tomography of breast and esophageal tissues benchmarked against histopathology. Histopathologists and radiologists could provide matching results of esophageal tumors examined at selected stages of intrusion [62]. For both breast and esophagus tissues, phase tomography data offered an enhanced capability for diagnosis over histology slices alone [62]. Hence, phase tomography complemented histopathology in clinical settings.

S. Singh *et al.* demonstrated the imaging power of phase tomography for weakly X-ray absorbing tissues in healthy and diseased murine ankles [63]. The spondylarthritis-induced inflammation in the form of swelling of the synovial membrane was visualized [63]. Furthermore, deep learning supported the segmentation of inflammatory tissues [63].

C.E. Lewis, N.A. Ives, and G.W. Stupian elucidated the challenges in tomography of objects with high aspect ratios including printed circuit boards [64]. They proposed computed laminography and focused their study on the inspection of fine features within a printed circuit board [64].

Microtomography has been especially powerful to characterize porous materials. D. Iuso *et al.* used conventional microtomography to evaluate the pores within objects built by selective laser melting [65]. To improve the segmentation of the pores, the authors applied machine learning algorithms [65].

L. Costeur *et al.* showed an impressive example of unique-object imaging using laboratory-based microtomography [66]. They imaged and compared a celluloid cast, maybe even the earliest prepared, with the digital counterpart of another petrosal bone of the same taxon from the same locality [66]. This study demonstrated the power of conventional microtomography in nondestructive evaluation of cultural heritage.

5. INTERDISCIPLINARY RESEARCH IN THE FIELD OF TOMOGRAPHY

The arrangement of the conference contributions in three pillars, *i.e.* hard X-ray tomography instrumentation; algorithms for reconstruction, artefact removal and data treatment; as well as the wide-spread use of the technique in medically

relevant applications and beyond, is to some extent arbitrary because many talks, posters, and papers include elements of two or in many cases even three pillars. This inclusion of instrumentation and algorithms into the envisioned and actual applications also becomes apparent from the author lists of researchers with diverse background. This spirit of teamwork spirit has been inherent throughout the conference series *Developments in X-Ray Tomography*.

This conference is known as the longest running non-clinical tomography conference. Contrary to many clinical conferences with proceedings that are a collection of extended abstracts, *Developments in X-Ray Tomography* is a 400-page book, which includes full papers with an average number of more than eight pages. Each paper has about 25,000 characters and has been reviewed by at least two independent reviewers. The review quality and efficiency has been guaranteed by the members of the Program Committee. Most of the 48 papers were revised according to the reviewer's feedbacks.

As pointed out previously [67], the proceedings volumes on *Developments in X-Ray Tomography* have been regarded as a bargain box for the interdisciplinary community working in the area of hard X-ray tomography and served as a periodic snapshot at a central place where contributions from many disciplines cross-fertilize.

ACKNOWLEDGEMENT

The author gratefully acknowledges the valuable input of Stuart R. Stock and Ge Wang.

REFERENCES

- [1] Stock, S. R., [MicroComputed Tomography: Methodology and Applications] CRC Press, (2019).
- [2] Migga, A., Schulz, G., Rodgers, G., Osterwalder, M., Tanner, C., Blank, H., Jerjen, I., Salmon, P., Twengström, W., Scheel, M., Weitkamp, T., Schlepütz, C. M., Bolten, J. S., Huwyler, J., Hotz, G., Madduri, S., and Müller, B., "Comparative hard x-ray tomography for virtual histology of zebrafish larva, human tooth cementum, and porcine nerve," *Journal of Medical Imaging (Bellingham)* **9**(3), 031507 (2022).
- [3] Rodgers, G., Sigran, G. R., Tanner, C., Hieber, S. E., Beckmann, F., Schulz, G., Scherberich, A., Jaquiéry, C., Kunz, C., and Müller, B., "Combining high-resolution hard X-ray tomography and histology for stem cell-mediated distraction osteogenesis," *Applied Sciences* **12**(12), 6286 (2022).
- [4] Schropp, A., Achilles, S., Patjens, S., Seiboth, F., Stückelberger, M., Jiang, Z., Pikul, J., and Schroer, C., "3D scanning coherent x-ray microscopy at PtyNAMI," *Proceedings of SPIE* **12242**, 1224208 (2022).
- [5] Doherty, A., Savidis, S., Astolfo, A., Massimi, L., Djurabekova, N., Navarrete Leon, C., Gerli, M. F., Iacoviello, F., Shearing, P., Norman, D., Williams, M., Olivo, A., and Endrizzi, M., "X-ray dark-field tomography using edge-illumination," *Proceedings of SPIE* **12242**, 1224209 (2022).
- [6] Liebi, M., [SAXS tensor tomography: 3D reciprocal space map reconstructions within 3D specimens] *SPIE*, 1224207 (2022).
- [7] Appel, C., Gao, Z., Etzold, B. J. M., Liebi, M., and Guizar-Sicairos, M., [Multiscale characterization of nanostructure and dynamic processes in nanoporous composite materials using a correlative approach with ptychographic X-ray tomography and scanning small-angle X-ray scattering] *SPIE*, 122420B (2022).
- [8] Nikitin, V., [Real-time micro-CT reconstruction with zooming to features of interest] *SPIE*, 122420C (2022).
- [9] Beckmann, F., Moosmann, J., Hammel, J., Wilde, F., Greving, I., Lottermoser, L., Riedel, M., Bidola, P., and Burmester, H., [Radiation dose optimized microtomography using synchrotron radiation at beamlines P05/PETRA III and P07/PETRA III] *SPIE*, 122420D (2022).
- [10] Kazimi, B., Heuser, P., Schluenzen, F., Cwieka, H., Krüger, D., Zeller-Plumhoff, B., Wieland, F., Hammel, J., Beckmann, F., and Moosmann, J., "An active learning approach for the interactive and guided segmentation of tomography data," *Proceedings of SPIE* **12242**, 122420F (2022).

- [11] Vo, N., Wang, H., Hu, L., Zhou, T., Zdora, M.-C., Deyhle, H., Atwood, R., and Drakopoulos, M., "Practical implementations of speckle-based phase-retrieval methods in Python and GPU for tomography," Proceedings of SPIE **12242**, 122420E (2022).
- [12] Ahmed, S., Deyhle, H., James, A., Le Houx, J., Garland, P., Drakopoulos, M., Reinhard, C., and Aslani, N., [DIAD: An instrument for dual imaging and diffraction at Diamond Light Source] SPIE, 122420G (2022).
- [13] Li, M., Bohacova, J., Uher, J., Cong, W., Rubinstein, J., and Wang, G., "Motion correction for robot-based x-ray photon-counting CT at ultrahigh resolution," Proceedings of SPIE **12242**, 122420Y (2022).
- [14] Vanthienen, P.-J., Sanctorum, J., Huyge, B., Six, N., Sijbers, J., and De Beenhouwer, J., "Alternative grating designs for cone-beam edge illumination x-ray phase contrast imaging," Proceedings of SPIE **12242**, 122420Z (2022).
- [15] Momose, A., Ueda, R., Cai, M., Zhao, Z., Kalirai, S., Stan, M., Irwin, J., Kawakami, H., Zangi, P., Meyer, P., Börner, M., and Schulz, J., "Recent progress in grating-based microscopic x-ray phase tomography," Proceedings of SPIE **12242**, 1224210 (2022).
- [16] Bech, M., "Dual-binary phase gratings for x-ray interferometry," Proceedings of SPIE **12242**, 1224211 (2022).
- [17] Yoneyama, A., "Three-dimensional x-ray thermography using crystal-based x-ray interferometer," Proceedings of SPIE **12242**, 122420X (2022).
- [18] Yoneyama, A., Baba, R., Takamatsu, D., Kamezawa, C., Inoue, I., Osaka, T., Owada, S., and Yabashi, M., "Feasibility study of interferometric phase-contrast X-ray imaging using the hard-X-ray free-electron laser of the SPring-8 Angstrom Compact Free-Electron Laser," Journal of Synchrotron Radiation **27**(5), 1358-1361 (2020).
- [19] Sanctorum, J., Six, N., Sijbers, J., and De Beenhouwer, J., "Augmenting a conventional x-ray scanner with edge illumination-based phase contrast imaging: how to design the gratings," Proceedings of SPIE **12242**, 1224218 (2022).
- [20] Bossuyt, C., De Beenhouwer, J., and Sijbers, J., "Optimization of a multi-source rectangular X-ray CT geometry for inline inspection," Proceedings of SPIE **12242**, 1224219 (2022).
- [21] Niu, C., Dasegowda, G., Yan, P., Kalra, M., and Wang, G., "Multi-view X-ray dissection improves nodule detection," Proceeding of SPIE **12242**, 1224217 (2022).
- [22] Karimi, S., and Tringe, J., "Cross-talk and spatial resolution in a CT scanner with a flat panel detector," Proceedings of SPIE **12242**, 122421A (2022).
- [23] Patil, B., Agrawal, U., Singhal, V., Langoju, R., Hsieh, J., Lakshminarasimhan, S., and Das, B., "Low performing pixel correction in computed tomography using deep learning," Proceedings of SPIE **12242**, 122420K (2022).
- [24] Gao, Q., and Shan, H., "CoCoDiff: A contextual conditional diffusion model for low-dose CT image denoising," Proceedings of SPIE **12242**, 122420I (2022).
- [25] Niu, C., Li, M., Guo, X., and Wang, G., "Self-supervised dual-domain network for low-dose CT denoising," Proceedings of SPIE **12242**, 122420H (2022).
- [26] Flenner, S., Hagemann, J., Storm, M., Kubec, A., Qi, P., David, C., Longo, E., Niese, S., Gawlitza, P., Zeller-Plumhoff, B., Reimers, J., Müller, M., and Greving, I., "Hard X-ray nanotomography at the P05 imaging beamline at PETRA III," Proceedings of SPIE **12242**, 122420L (2022).
- [27] Achilles, S., Ehrig, S., Hoffmann, N., Kahnt, M., Becher, J., Fam, Y., Sheppard, T., Brückner, D., Schropp, A., and Schroer, C., "GPU-accelerated coupled ptychographic tomography," Proceedings of SPIE **12242**, 122420N (2022).
- [28] Andrew, M., Andreyev, A., Yang, F., Terada, M., Gu, A., and White, R., "Fully automated deep learning-based resolution recovery," Proceedings of SPIE **12242**, 122420M (2022).
- [29] Six, N., Renders, J., De Beenhouwer, J., and Sijbers, J., "Joint reconstruction of attenuation, refraction and dark field x-ray phase contrasts using split Barzilai-Borwein steps," Proceedings of SPIE **12242**, 122420O (2022).
- [30] Li, S., French, M., Pavlov, K., and Li, H. T., "Shallow U-Net deep learning approach for phase retrieval in propagation-based phase-contrast imaging," Proceedings of SPIE **12242**, 122421Q (2022).

- [31] Müller, B., Deyhle, H., Lang, S., Schulz, G., Bormann, T., Fierz, F., and Hieber, S., "Three-dimensional registration of tomography data for quantification in biomaterials science," *International Journal of Materials Research* **103**(2), 242-249 (2012).
- [32] Tanner, C., Müller, B., and Rodgers, G., "Registration of microtomography images: Challenges and approaches," *Proceedings of SPIE* **12242**, 122420T (2022).
- [33] Tekawade, A., Nikitin, V., Satapathy, Y., Liu, Z., Zhang, X., Kenesei, P., De Carlo, F., Kettimuthu, R., and Foster, I., [A real-time porosity mapping solution for synchrotron micro-CT of large 3D printed parts] *SPIE*, 122420U (2022).
- [34] Wieczorek, M., Schaff, F., Pfeiffer, F., and Lasser, T., "Anisotropic X-ray dark-field tomography: A continuous model and its discretization," *Physical Review Letters* **117**(15), 158101 (2016).
- [35] Huyge, B., Jeurissen, B., De Beenhouwer, J., and Sijbers, J., "Fiber orientation estimation by constrained spherical deconvolution of the anisotropic edge illumination x-ray dark field signal," *Proceedings of SPIE* **12242**, 122420V (2022).
- [36] Paramonov, P., Renders, J., Elberfeld, T., De Beenhouwer, J., and Sijbers, J., "Efficient X-ray projection of triangular meshes based on ray tracing and rasterization," *Proceeding of SPIE* **12242**, 122420W (2022).
- [37] Andreyev, A., Yang, F., Andrew, M., Omlor, L., and Villarraga-Gómez, H., "Spatially variant optimization of an empirical beam-hardening correction algorithm," *Proceedings of SPIE* **12242**, 122421G (2022).
- [38] Li, M., Cooley, V., Nikitin, V., Stock, S., and Wang, G., "Metal pin artifact reduction with masked iterative nano-CT reconstruction," *Proceedings of SPIE* **12242**, 122421H (2022).
- [39] Nguyen, A. T., Renders, J., Soete, J., Wevers, M., Sijbers, J., and De Beenhouwer, J., "An accelerated motion-compensated iterative reconstruction technique for dynamic computed tomography," *Proceedings of SPIE* **12242**, 122421F (2022).
- [40] Sushmit, A., Xu, Y., Mariani, O., Lyu, Q., Li, Y., Cao, X., Wiedeman, C., Ma, H., Maltz, J., Yu, H., and Wang, G., "A data generation pipeline for cardiac vessel segmentation and motion artifact grading," *Proceedings of SPIE* **12242**, 122421J (2022).
- [41] Kuo, W., Le, N. A., Spingler, B., Schulz, G., Müller, B., and Kurtcuoglu, V., "Tomographic imaging of microvasculature with a purpose-designed, polymeric x-ray contrast agent," *Proceedings of SPIE* **12242**, 1224205 (2022).
- [42] Dreier, T., Bernström, G., Ganji, S., Norvik, C., Tran-Lundmark, K., and Bech, M., "Radiopaque dyes allow vessel imaging in lung tissue using laboratory phase contrast micro-CT," *Proceedings of SPIE* **12242**, 1224203 (2022).
- [43] Reichmann, J., Ruhwedel, T., Möbius, W., and Salditt, T., "Neodymium acetate as a contrast agent for x-ray phase-contrast tomography," *Proceedings of SPIE* **12242**, 1224204 (2022).
- [44] Taphorn, K., Busse, M., Brantl, J., Günther, B., Diaz, A., Holler, M., Dierolf, M., Pfeiffer, F., and Herzen, J., "Investigation of X-ray stains with near-field ptychographic computed tomography," *Proceedings of SPIE* **12242**, 1224206 (2022).
- [45] Humbel, M., Scheel, M., Tanner, C., Rodgers, G., Schulz, G., Carlucci, C., von Jackowski, J., Sigran, G., Izquierdo, A., Weitkamp, T., and Müller, B., "Nano-tomography of dental composites with wide color matching," *Proceeding of SPIE* **12242**, 122420Q (2022).
- [46] von Jackowski, J., Müller, B., Schulz, G., Hotz, G., Weitkamp, T., Wittwer-Backofen, U., and Tanner, C., "Tomographic imaging of unique objects: annual layers in tooth cementum of Anna Catharina Bischoff born 1719," *Proceedings of SPIE* **12242**, 122421O (2022).
- [47] Velasco, A., Tanner, C., Schulz, G., Rodgers, G., von Jackowski, J., Humbel, M., Weitkamp, T., Bunn, H., and Müller, B., "Hierarchical imaging of African bovid tooth cementum using X-ray microtomography," *Proceedings of SPIE* **12242**, 122420R (2022).
- [48] Stock, S., Cooley, V., Tribuzio, C., Li, L., Nikitin, V., and Antipova, O., "Growth bands in dogfish spines," *Proceedings of SPIE* **12242**, 122420S (2022).

[49] Schulz, G., Rodgers, G., Tanner, C., Weitkamp, T., Barbero, A., Wolf, F., Beer, D., and Müller, B., "Three-dimensional imaging of porcine joints down to the subcellular level," *Proceedings of SPIE* **12242**, 1224215 (2022).

[50] Lareida, A., Beckmann, F., Schrott-Fischer, A., Glueckert, R., Freysinger, W., and Müller, B., "High-resolution X-ray tomography of the human inner ear: synchrotron radiation-based study of nerve fibre bundles, membranes and ganglion cells," *Journal of microscopy* **234**(1), 95-102 (2009).

[51] Richter, C.-P., Young, H., Richter, S. V., Smith-Bronstein, V., Stock, S. R., Xiao, X., Soriano, C., and Whitlon, D. S., "Fluvastatin protects cochleae from damage by high-level noise," *Scientific Reports* **8**(1), 3033 (2018).

[52] Mennecart, B., Dziomber, L., Aiglstorfer, M., Bibi, F., DeMiguel, D., Fujita, M., Kubo, M. O., Laurens, F., Meng, J., Métais, G., Müller, B., Ríos, M., Rössner, G. E., Sánchez, I. M., Schulz, G., Wang, S., and Costeur, L., "Ruminant inner ear shape records 35 million years of neutral evolution," *Nature Communications*, in press (2022).

[53] Glückert, R., Rask-Andersen, H., Sergi, C., Schmutzhard, J., Müller, B., Beckmann, F., Rittinger, O., Schrott-Fischer, A., and Janecke, A., "Histology and synchrotron radiation based microtomography of the inner ear in a molecularly confirmed case of CHARGE syndrome" *American Journal of Medical Genetics Part A* **152**(3), 665-673 (2010).

[54] Müller, B., Bernhardt, R., Weitkamp, T., Beckmann, F., Bräuer, R., Schurigt, U., Schrott-Fischer, A., Glueckert, R., Ney, M., Beleites, T., Jolly, C., and Scharnweber, D., "Morphology of bony tissues and implants uncovered by high-resolution tomographic imaging" *International Journal of Materials Research* **98**(7), 613-621 (2007).

[55] Schaeper, J., Liberman, M. C., and Salditt, T., "Imaging of excised cochleae by micro-CT: staining, liquid embedding, and image modalities," *Proceeding of SPIE* **12242**, 1224214 (2022).

[56] Riedel, M., Hammel, J., Moosmann, J., Beckmann, F., Schwarzenberg, F., Schuetz, P., Henne, S., Wülfing, C., Busse, M., and Herzen, J., "Quantitative phase-contrast x-ray micro CT for visualization of mouse lymph nodes," *Proceedings of SPIE* **12242**, 1224213 (2022).

[57] Romell, J., Fernández Moro, C., Twengström, W., Larsson, J., Sparreli, E., Björnstedt, M., and Hertz, H., [X-ray phase-contrast CT as a complementary histology method] *SPIE*, 1224212 (2022).

[58] Rodgers, G., Tanner, C., Schulz, G., Weitkamp, T., Scheel, M., Girona Alarcón, M., Kurtcuoglu, V., and Müller, B., "Mosaic microtomography of a full mouse brain with sub-micron pixel size," *Proceedings of SPIE* **12242**, 122421L (2022).

[59] Croton, L. C. P., Morgan, K. S., Paganin, D. M., Kerr, L. T., Wallace, M. J., Crossley, K. J., Miller, S. L., Yagi, N., Uesugi, K., Hooper, S. B., and Kitchen, M. J., "In situ phase contrast X-ray brain CT," *Scientific Reports* **8**(1), 11412 (2018).

[60] Croton, L. C. P., Ruben, G., Morgan, K. S., Paganin, D. M., and Kitchen, M. J., "Ring artifact suppression in X-ray computed tomography using a simple, pixel-wise response correction," *Opt. Express* **27**(10), 14231-14245 (2019).

[61] Croton, L., Crossley, K., McDonald, C., Morgan, K., Penny, T., Galinsky, R., Hooper, S., Ruben, G., Pollock, J., Schaff, F., Croughan, M., Sutherland, A., and Kitchen, M., "Pre-clinical phase-contrast imaging of the whole brain in situ: from traumatic to diffuse white matter injury," *Proceedings of SPIE* **12242**, 122421B (2022).

[62] Partridge, T., Massimi, L., Wolfson, P., Jiang, J., Astolfo, A., Suaris, T., Havariyoun, G., Savvidis, S., Maughan Jones, C. J., Djurabekova, N., Sam Hawker, P. M., Smit, B., Larkin, O. J., Millard, E., Shorrock, W., Waltham, R. M., Ho, K. M. A., Mc Bain, H., Wilson, A., Peel, A., Shah, Z., Nelan, R. L., Delaney, H., Liyadipita, A., Lavine, A. P., Dawas, K., Mohammadi, B., Qureshi, Y. A., Chouhan, M. D., Taylor, S. A., Mughal, M., Endrizzi, M., Hagen, C. K., Munro, P. R. T., Duffy, S. W., Jones, J. L., Novelli, M., Lovat, L. B., Haig, I. G., Bate, D., and Olivo, A., "Intra-operative assessment of cancer with x-ray phase contrast computed tomography," *Proceedings of SPIE* **12242**, 122421C (2022).

- [63] Singh, S., Romand, X., Broche, L., Favier, B., Baillet, A., and Brun, E., "Evaluating inflammations in high-resolution x-ray phase contrast images of SKG spondylarthritis mice models," Proceeding of SPIE **12242**, 122421E (2022).
- [64] Lewis, C., Ives, N., and Stupian, G., "Cone-beam computed laminography for flexible three-dimensional analysis of stacked microvias in multilayer printed circuit boards," Proceedings of SPIE **12242**, 122421D (2022).
- [65] Iuso, D., Chatterjee, S., Heylen, R., Cornelissen, S., De Beenhouwer, J., and Sijbers, J., "Evaluation of deeply supervised neural networks for 3D pore segmentation in additive manufacturing," Proceedings of SPIE **12242**, 122421K (2022).
- [66] Costeur, L., Mennecart, B., Orliac, M., and Schulz, G., "Science history meets microtomography: Comparison of the world's oldest physical model of an extinct animal's inner ear with the 3D virtual counterpart," Proceedings of SPIE **12242**, 122421N (2022).
- [67] Müller, B., "Emerging developments in tomographic imaging with hard X rays," Proceeding of SPIE **11840**, 1184004 (2021).